Biochimica et Biophysica Acta 1838 (2014) 1529–1535

Contents lists available at ScienceDirect

Biochimica et Biophysica Acta

journal homepage: www.elsevier.com/locate/bbamem

Multi-step formation of a hemifusion diaphragm for vesicle fusion revealed by all-atom molecular dynamics simulations ☆

Hui-Hsu Gavin Tsai *, Che-Ming Chang, Jian-Bin Lee

Department of Chemistry, National Central University, Jhong-Li City, Tao-Yuan County 32001, Taiwan

ARTICLE INFO

Article history:
Received 1 September 2013
Received in revised form 4 January 2014
Accepted 11 January 2014
Available online 24 January 2014

Keywords:
Membrane fusion
Hemifusion diaphragm
Multi-step event
Energy landscape
Hemifusion diaphragm thinning

ABSTRACT

Membrane fusion is essential for intracellular trafficking and virus infection, but the molecular mechanisms underlying the fusion process remain poorly understood. In this study, we employed all-atom molecular dynamics simulations to investigate the membrane fusion mechanism using vesicle models which were pre-bound by inter-vesicle Ca^{2+}-lipid clusters to approximate Ca^{2+}-catalyzed fusion. Our results show that the formation of the hemifusion diaphragm for vesicle fusion is a multi-step event. This result contrasts with the assumptions made in most continuum models. The neighboring hemifused states are separated by an energy barrier on the energy landscape. The hemifusion diaphragm is much thinner than the planar lipid bilayers. The thinning of the hemifusion diaphragm during its formation results in the opening of a fusion pore for vesicle fusion. This work provides new insights into the formation of the hemifusion diaphragm and thus increases understanding of the molecular mechanism of membrane fusion. This article is part of a Special Issue entitled: Membrane Structure and Function: Relevance in the Cell's Physiology, Pathology and Therapy.

1. Introduction

Membrane fusion is an essential event for intracellular trafficking, fertilization, recycling, and neurotransmitter release [1,2]; it is also a critical step for viral infection. Membrane fusion can be driven by fusion proteins, such as soluble *N*-ethylmaleimide–sensitive factor attachment protein receptor (SNARE) synaptotagmin. In protein-induced membrane fusion, specialized fusion proteins bind to membranes and bring the membranes together regulating content mixing and expanding the fusion pore [2]. Membrane fusion can also occur without the presence of a fusion protein in which case it is usually driven by membrane tension [3,4], pH [5], temperature, the lipid composition of the membrane [6], and cation binding [7–10]. According to the stalk hypothesis [1,11], fusion proceeds through the sequential merger of lipid leaflets from a membrane pair starting with the initial contact of the outer leaflets of the membrane pair, followed by stalk formation, formation of an expanded hemifused state, and opening of a fusion pore. In the stalk state, lipids from the proximal (outer) leaflets of a membrane pair are merged and the distal (inner) leaflets are separated. This stalk state can expand to form a hemifused state that features a hemifused diaphragm between distal (inner) leaflets of a membrane pair. The hemifused diaphragm (HD) can be opened forming a fusion pore that allows lipid mixing and content release.

Many studies have explored the mechanism underlying membrane fusion using various molecular simulation techniques in conjunction with different membrane models [5,6,12–16]. Significant new events in membrane fusion have recently been revealed. A transition state before the formation of stalk state has been identified by committor analysis from million-atom vesicle fusion simulations [17]; this transition state is characterized as the protrusion of a few hydrophobic tails into the hydrophilic interface from a vesicle pair. Using a coarse-grained model in conjunction with a planar lipid bilayer model at low hydration level, Knecht and colleagues also suggested that a similar higher energy state called a pre-stalk transition state exists prior to the fusion stalk formation [16]. Formation of this pre-stalk transition state requires energy to drive lipid tails splaying from the interior region of pairs of vesicles or planar lipid bilayers. We also observed this pre-stalk transition state in our recent all-atom molecular dynamics simulation of micelle fusion in the presence of Ca^{2+} ions [8]. Moreover, the Ca^{2+} ions were able to destabilize the micelles and promote the formation of this pre-stalk transition state. The pre-stalk transition state is not considered in most continuum models [18–20].

Whether the fusion process requires the formation of an equilibrium HD or not also remains controversial. In the hemifused state, only the outer leaflets of a membrane pair are fused, while the inner leaflets engage forming a new lipid bilayer referred to as the HD. In a coarse-grained molecular dynamics (MD) simulation of mixed PC/PE vesicle fusion, two fusion pathways have been observed [13]. One follows the so-called stalk-pore fusion mechanism, in which the stalk, expanded HD, and fusion pore are formed sequentially. In the other pathway, the pore forms after the formation of a "banana-shaped" stalk state. Ensemble MD simulations show that the first pathway with the formation of

☆ This article is part of a Special Issue entitled: Membrane Structure and Function: Relevance in the Cell's Physiology, Pathology and Therapy.

* Corresponding author. Tel.: +886 3 4227151x65909; fax: +886 3 4227664.
E-mail address: hhtsai@cc.ncu.edu.tw (H.-H.G. Tsai).

0005-2736/$ – see front matter © 2014 Elsevier B.V. All rights reserved.
http://dx.doi.org/10.1016/j.bbamem.2014.01.018

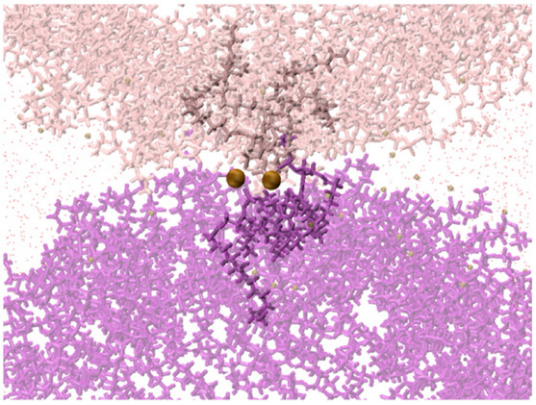

Fig. 1. Graph representing the initial contact of two vesicles bound together with inter-vesicle Ca^{2+}-lipid clusters. The inter-vesicle Ca^{2+}-lipid clusters are highlighted (Ca^{2+} cations are shown in van der Waals (VDW) style and the lipids are shown in licorice style).

the HD intermediate is the predominant of the two [12]. An energy barrier was observed for the nucleation of a small hemifused membrane segment in the vesicle-planar membrane fusion simulations [21].

In this study, we employed all-atom molecular dynamics simulations in conjunction with a vesicle model to investigate the molecular mechanism of vesicle fusion. We focused on the formation of the hemifusion diaphragm and its structure. We found that the formation of hemifusion diaphragm is not a continuous event, but rather, a multi-step event. The structure of the hemifusion diaphragm was investigated.

2. Computational methods

Each vesicle was composed of 357 1-palmitoyl 2-oleoyl phosphatidylethanolamine (POPE) lipids with 98 lipids making up the inner leaflet and 259 lipids making up the outer leaflet; the ratio of inner lipid number to the total lipid number is 27% [22]. The chemical structure and labeling of atoms of the POPE lipid are shown in Figure SI. Individual vesicles were first equilibrated in water using the TIP3P explicit solvent model [23] by a 50 ns MD simulation. Pairs of vesicles were bound together with the pre-formed inter-vesicle Ca^{2+}-lipid clusters [9,24,25] solvated in TIP3P water with 150 mM $CaCl_2$ (Fig. 1). Six MD simulations of vesicle fusion were performed using different initial configurations and velocities. The details of the simulations and the nomenclature of the simulation systems are summarized in Table 1.

All the MD simulations were performed using the CHARMM36 [26] all-atom force field and in parallel using MD NAMD 2.7b3 software [27] with an NPT ensemble under three-dimensional periodic boundary conditions. The simulation temperature was controlled to 310 K by Langevin dynamics and the pressure was controlled to 1 bar using the Langevin piston Nosé–Hoover method [28]; the three orthogonal dimensions of the periodic cell were changed independently. Cutoffs of 12.0 and 13.5 Å were used to calculate the pairwise interactions and generate a list of neighboring atom pairs, respectively. The non-bonded neighbor list was updated every 10 steps. The particle-mesh Ewald summation technique was used to count the long-range electrostatic interactions. The force switching function [29] was applied to smooth the nonbonded electrostatics and van der Waals potential energy when the inter-nuclear distance for two atoms was between 9 and 12.0 Å. The covalent bond lengths involving hydrogen atoms were constrained by the SHAKE algorithm [30] which allows the use of an integration timestep of 2 fs. Prior to production runs, each simulation system was energy-minimized using a conjugate gradient algorithm to remove the bad contacts of the initial configuration. All simulated systems reached an energy tolerance of 0.0001 kcal/mol after 100,000 minimization steps. A 0.1-ns slow heating simulation was then performed until the system temperature reached 310 K. The trajectories were recorded every 5 ps.

Several properties were calculated. Inter-vesicle contact to measure the degree of vesicle fusion was calculated using 4 different methods according to the following criteria. Two heavy atoms located on different vesicles were considered to be one contact when their distance was shorter than 5 Å. This cutoff was chosen based on the radial distribution function (RDF) of heavy atoms in a single vesicle, by which the first peak was covered. The same method was used to calculate the contact numbers of water molecules inside individual vesicles. To estimate the degree of exposure of the lipid tails, we calculated the solvent-accessible surface area (SASA) using the approach described by Lee et al. [31]. The lipid tails of POPE were defined as extending from C_{34} to C_{316} in Sn-1 and from C_{24} to C_{218} in Sn-2. These aliphatic carbon atoms were originally buried to a greater extent inside the vesicle based on the atom distribution analysis of the simulation of the single vesicle. The method used to calculate the number of water molecules between two vesicles (N_W) is described in detail in our previous work [8]; instead, a square with sides of 70 Å, slightly smaller than the diameter of a vesicle (ca. 100 Å) was used. We calculated the value of $g(r)$, which is useful for describing the structures of two chosen atoms in a given system, using the expression

$$g(r) = \frac{N(r)}{4\pi r^2 \rho \delta r}$$

where $N(r)$ is the number of two chosen atoms at a distance r, δr is a spherical shell of thickness at a distance r of two chosen atoms, and ρ is the number density. All analyses were performed using Pine-MD, an in-house program developed by our group that has been employed in previous MD studies of the structural and dynamic properties of lipid bilayers [24,25], and the molecular mechanism of micelle fusion [8].

Table 1
Names, compositions, and simulation times of the studied systems.

System name	Atoms	POPE (Inner/outer)[a]	Water (Inside/outside)[b]	Ca^{2+} (Inside/outside)[b]	Cl^- (Inside/outside)[b]	Simulation time (ns)	Results
Single vesicle system							
1V-POPE-Ca^{2+}-SysI	283398	98/259	804/78573	2/212	4/424	40	Equilibrium
Two vesicle system							
2V-POPE-Ca^{2+}-SysI	465231	98/259	803/123382	2/335	4/670	180	Hemifused
2V-POPE-Ca^{2+}-SysII	451833	98/259	803/118921	2/330	4/660	130	Fused
2V-POPE-Ca^{2+}-SysIII	465084	98/259	803/123333	2/335	4/670	130	Fused
2V-POPE-Ca^{2+}-SysIV	529317	98/259	804/144686	2/391	4/782	105	Fused
2V-POPE-Ca^{2+}-SysV	451683	98/259	803/118877	2/324	4/648	100	Unfused
2V-POPE-Ca^{2+}-SysVI	529428	98/259	804/144723	2/391	4/782	100	Fused

[a] Inner leaflet/outer leaflet POPE lipid number per vesicle.
[b] Components located inside one vesicle/outside the vesicle(s).

3. Results and discussion

We performed all-atom MD simulations to investigate membrane fusion using vesicle models composed of POPE lipids. Vesicle pairs were first bound together with pre-formed inter-vesicle Ca^{2+}-lipid clusters [9,24,25] to approximate Ca^{2+}-catalyzed fusion. Six simulations were performed using different initial configurations and velocities. We observed spontaneous fusion within a 100-ns simulation for five of the six simulations. Here, we present the 2V–POPE–Ca^{2+}–SysI in detail as a framework for general fusion events. The other systems are presented in summary, highlighting the differences between them and the 2V–POPE–Ca^{2+}–SysI.

3.1. Structural characteristics of fusion events

To understand the structural characteristics of vesicle fusion and transformation, we calculated six parameters of the 2V-POPE-Ca^{2+} system as a function of the simulation time (Fig. 2): contact numbers of inner lipids–inner lipids of vesicle pairs ($N_{C\text{-}in}$) and outer lipids–outer lipids of vesicle pairs ($N_{C\text{-}out}$), four different types of SASA for lipid tails, inter-vesicle water numbers (N_W), and contact numbers of inner water molecules from individual vesicles ($N_{C\text{-}wat}$). The four different types of SASA are: (*i*) the total SASA of the inner lipid tails of two vesicles ($SASA_{tot\text{-}in}$), calculated by taking two vesicles into consideration at the same time; (*ii*) the sum of the SASA of each vesicle's inner lipid tails ($SASA_{sum\text{-}in}$), where the SASA of each vesicle's inner lipid tails was calculated individually without considering the other vesicle; (*iii*) the total SASA of the outer lipid tails of two vesicles ($SASA_{tot\text{-}out}$), calculated by taking two vesicles into consideration at the same time; and (*iv*) the sum of the SASA of each vesicle's outer lipid tails ($SASA_{sum\text{-}out}$), where the SASA of each vesicle's outer lipid tails was calculated individually without considering the other vesicle.

The six vertical dashed lines in Fig. 2 indicate the various fusion events: the orange dashed line indicates the initial time that a stable stalk state was formed; the black dashed line indicates the time when a stable stalk state had been formed; the blue dashed line indicates the initial time of the formation of a stable hemifused state; the green dashed line indicates the initial time of the pore formation; the magenta dashed line indicates the initial time of the formation of the fused state and; the purple dashed line indicates the time when a stable fused state

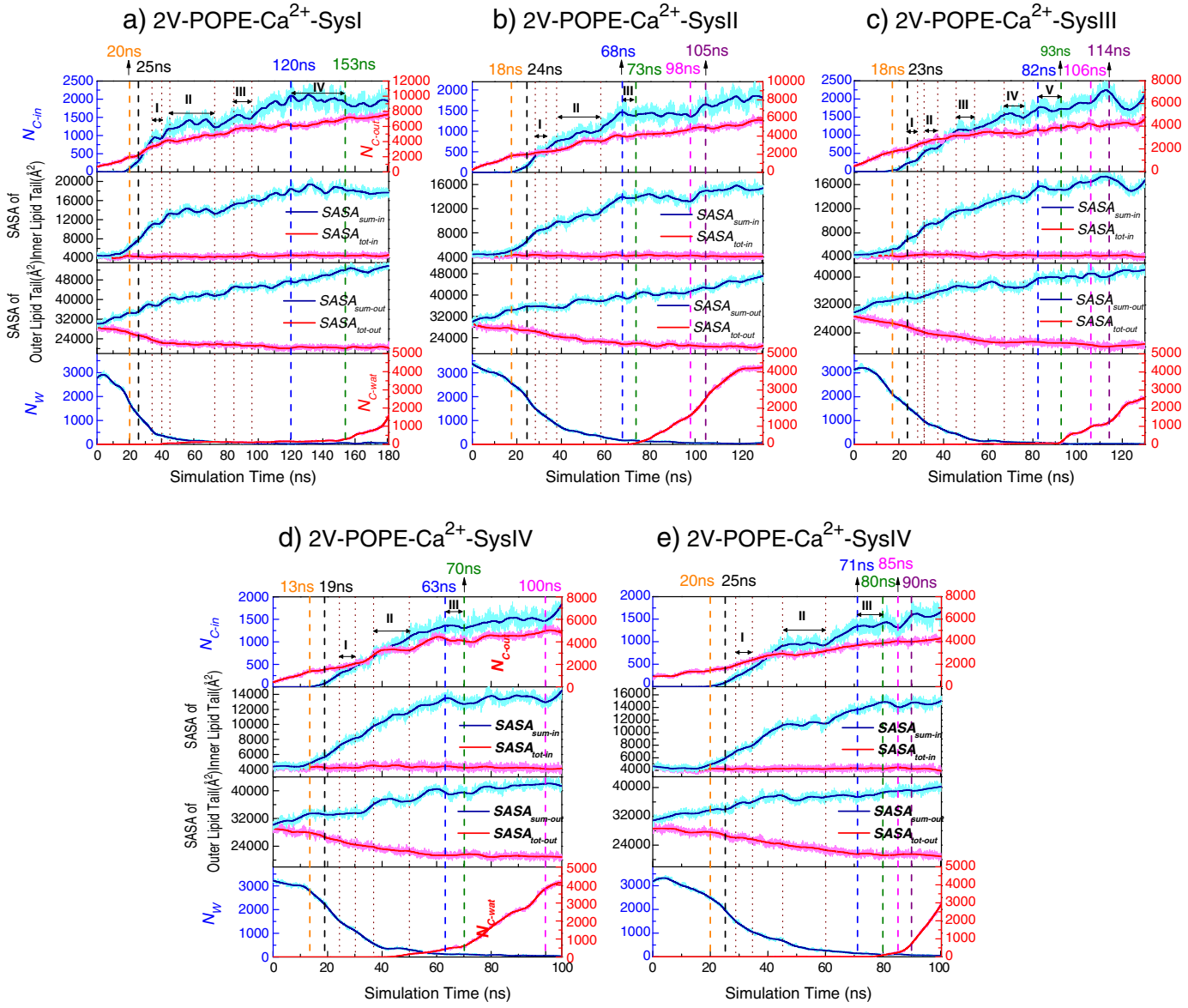

Fig. 2. Six structural properties of vesicle fusion of 2V–POPE–Ca^{2+} systems that evolve over simulation time. For explanations of the properties and the vertical lines, see the text.

was formed. In addition, several vertical dotted lines and arrows in Fig. 2 indicate the time periods of the stable hemifused states. Each stable hemifused state is also labeled with a Roman numeral. These time points and their corresponding states were mainly determined from the trends in the values of $N_{C\text{-}in}$, $SASA_{sum\text{-}in}$, $N_{C\text{-}out}$, and $SASA_{sum\text{-}out}$ and the free energy landscape (see Section 3.2). They were further validated by visualizing the structures of simulated trajectories using VMD software [32].

In the 2V–POPE–Ca^{2+}–SysI simulation, the $SASA_{sum\text{-}out}$ value increased from 0 to 20 ns and then slowed down thereafter. Of note, the $SASA_{sum\text{-}out}$ value remains at a similar level between 20 and 25 ns. A similar tendency is observed for the $N_{C\text{-}out}$ values. These results indicate that the lipid tails of the outer leaflets from two individual vesicles are in contact and the contacting structure remains stable from 20–25 ns. We, therefore, characterize the structure during this time period as a stalk state.

After 153 ns (marked by the green dashed line), the contact number of inner water molecules of two individual vesicles ($N_{C\text{-}wat}$) dramatically increases indicating the formation of a fusion pore. During the time period between 25 ns (stalk state) and 153 ns (formation of fusion pore), the $SASA_{sum\text{-}in}$, $SASA_{sum\text{-}out}$, $N_{C\text{-}in}$ and $N_{C\text{-}out}$ values generally increase with simulation time. Nevertheless, during some specific time periods, we observed that the $SASA_{sum\text{-}in}$, and $N_{C\text{-}in}$ values remain at a similar level. The contact of the inner lipids of two individual vesicles indicated by the $SASA_{sum\text{-}in}$, and $N_{C\text{-}in}$ values is a structural characteristic of the hemifusion diaphragm. Half of the $SASA_{sum\text{-}in}$ can be considered as the area of the hemifusion diaphragm [17]. Thus, we characterize the structure during this time period as the hemifusion diaphragm. For the 2V–POPE–Ca^{2+}–SysI, we characterized four hemifusion states (marked with Roman numerals): hemifused state I remains stable for approximately 6 ns between 33.5 and 39.5 ns; it starts to form 8.5 ns after the formation of the stable stalk state (25 ns). After 39.5 ns, the $SASA_{sum\text{-}in}$, and $N_{C\text{-}in}$ values start to increase and reach a similar level between 47.7 and 72.6 ns (hemifused state II; stable for 27.9 ns). After 72.6 ns, the $SASA_{sum\text{-}in}$, and $N_{C\text{-}in}$ values start to increase again and reach a similar level during the period between 84.3 and 96.1 ns (hemifused state III; stable for 11.8 ns). Similarly, the $SASA_{sum\text{-}in}$, and $N_{C\text{-}in}$ values start to remain at a similar level at 120 ns and the fusion pore forms at 153 ns. We define the time period between 120 and 153 ns as hemifused state IV. The size of the hemifusion diaphragm increases with time indicated by the increased $SASA_{sum\text{-}in}$, and $N_{C\text{-}in}$ values. Similarly, more than two hemifused states were observed for other simulation systems. These results show that the formation of the hemifusion diaphragm is not a continuous event, but rather a multi-step process.

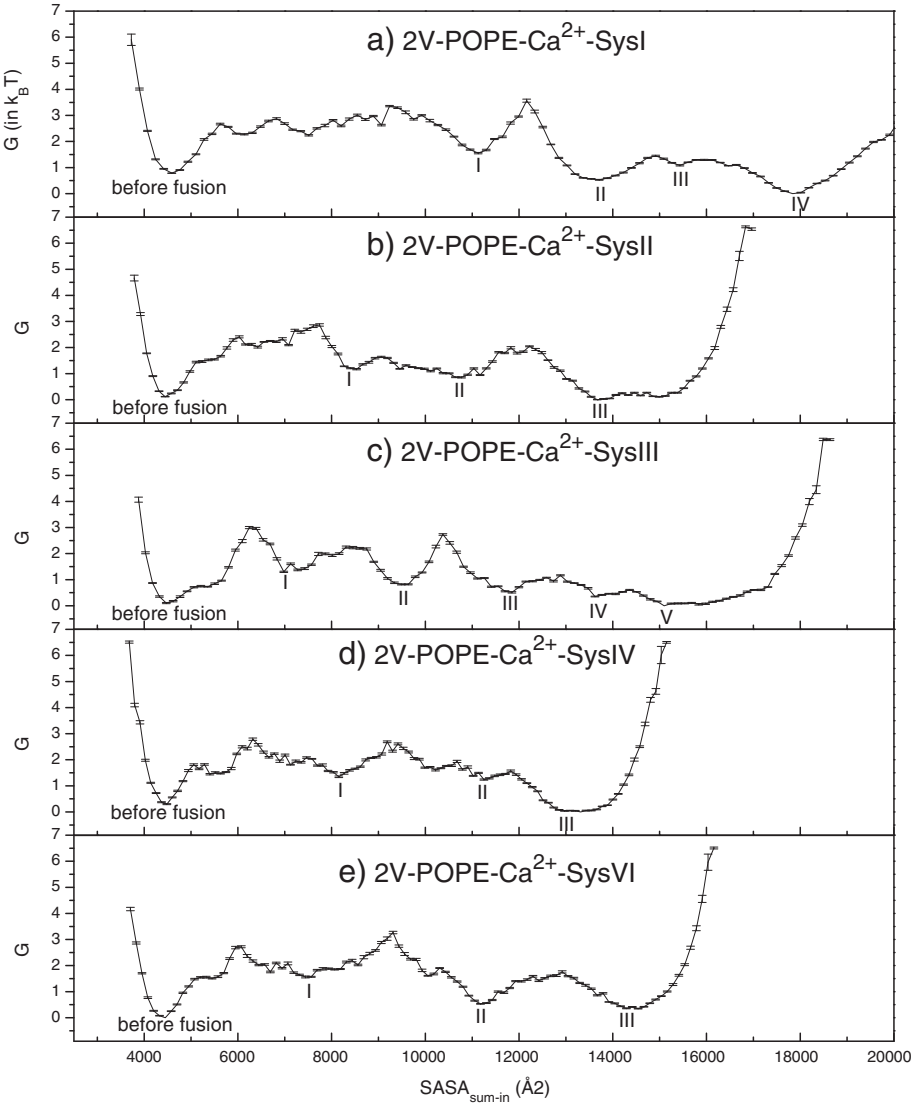

Fig. 3. One dimensional free energy profile of a hemifusion diaphragm formation at 310 K. The free energy profile is plotted in terms of the value of $SASA_{sum\text{-}in}$ (Å^2). The units of free energy are given in multiples of k_BT.

In general, the $SASA_{sum\text{-}in}$ and $SASA_{sum\text{-}out}$ values increase with simulation time; however, $SASA_{tot\text{-}in}$ remains at constant low values and the $SASA_{tot\text{-}out}$ values decrease slightly with time. These results imply that the exposed lipid tails of one vesicle were hindered by the other vesicle and *vice versa*. The inter-vesicle water molecules were almost expelled out from the inter-vesicular regions after a stable hemifused state I was formed.

Increasing evidence suggests that intermediate structures with negative values of a local monolayer curvature are required for membrane fusion [33,34]. Recent membrane simulation reveals that a decrease in pH results in decreased area per lipid, increased membrane thickness, and increased order parameter of the lipid hydrocarbon chains [5]. Furthermore, the results show that the value of spontaneous curvature in a membrane shifts in the negative direction with decreasing pH formed solely of lysophosphatidylcholines and free fatty acids. Our previous study [25] of lipid bilayers in various cations show that the Ca^{2+} ions by forming Ca^{2+}-lipid clusters [5] can induce similar structural changes to those observed in the acidic environment. Therefore, it is expected that Ca^{2+} ions can also induce the negative curvature of lipid micelles [8] as well as the lipid vesicles in this study and that this negative curvature may be involved in the membrane fusion process.

3.2. Multi-step formation of hemifusion diaphragm

The states labeled with Roman numerals in Fig. 2 are characterized by their stable $SASA_{sum\text{-}in}$ and $N_{C\text{-}in}$ values, obvious structural features of the hemifusion diaphragm. To further characterize the hemifusion states, we projected the trajectories on one reaction coordinates—the value of $SASA_{sum\text{-}in}$—in terms of the potential mean force (Fig. 3). We calculated the free energy using the equation

$$\Delta G(q) = -k_B T \ln P(q)$$

where q is the value of $SASA_{sum\text{-}in}$ and $P(q)$ is a canonical probability distribution function; the lowest free energy was set to zero. To assess whether the simulations were sufficient to calculate such an energy profile, we performed a cross validation procedure using a jackknifing approach [35]. We randomly removed 10% of the trajectories at a time and recalculated the free energy profile. We thus obtained ten resulting sets of free energy profiles (nine sets had 10% trajectories removed, one set was the original one) and calculated their standard deviations. The standard deviations are labeled in Fig. 3. It can be seen from Fig. 3 that the standard deviations are much smaller than their corresponding free energies, indicating that the simulations were sufficient to calculate the energy profile. Fig. 3 shows some local energy minima labeled with Roman numerals, which correspond to the hemifusion states labeled in Fig. 2. For a given system, all neighboring local energy minima are separated by an energy barrier. These results further suggest that the formation of a hemifusion diaphragm for vesicle fusion is a multi-step process.

To investigate the mechanism of hemifusion diaphragm formation in more detail, we projected the trajectories of the 2V–POPE–Ca^{2+}

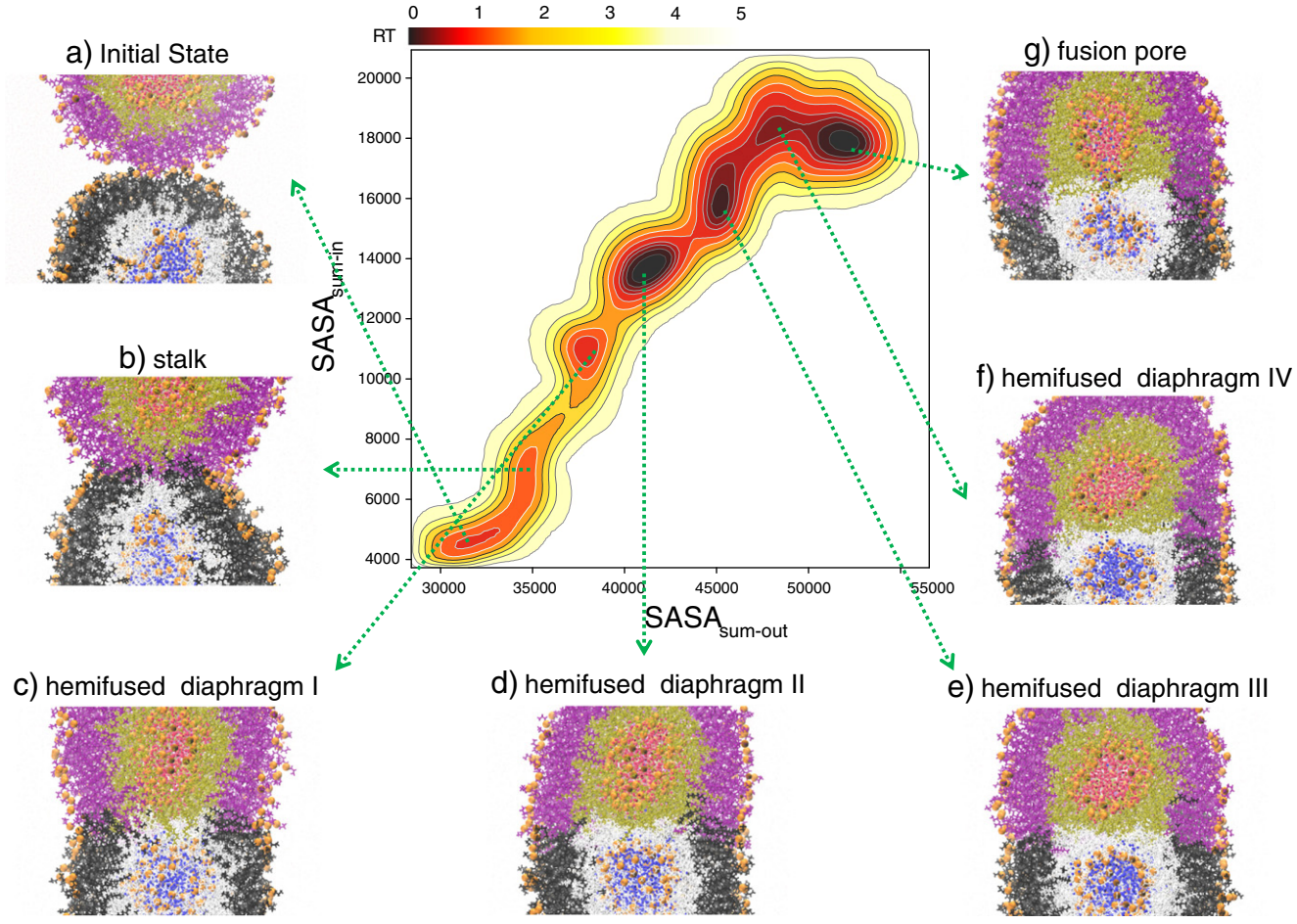

Fig. 4. Two dimensional free energy landscape of vesicle fusion at 310 K. The free energy landscape is plotted in terms of the values of $SASA_{sum\text{-}out}$ and $SASA_{sum\text{-}in}$ (Å^2). The units of free energy are given in multiples of k_BT. Representative snapshots of each local energy minimum are provided beside the plot: (a) unfused state; (b) stalk state; (c) hemifused state I; (d) hemifused state II; (e) hemifused state III; (f) hemifused state IV; and (g) fusion pore. Color code: The phosphorus atoms are displayed in orange using the VDW style. The outer leaflets of two fusing vesicles are presented in licorice style in purple and black, respectively. The inner leaflets of two fusing vesicles are presented in the licorice style in gold and white, respectively. For clarity, the water molecules are presented as oxygen atoms only using CPK style; the water molecules inside the vesicles are shown in red and blue, respectively.

Table 2
The average thickness of hemifusion diaphragm.

State	Simulations systems				
	2V-POPE-Ca^{2+}-SysI	2V-POPE-Ca^{2+}-SysII	2V-POPE-Ca^{2+}-SysIII	2V-POPE-Ca^{2+}-SysIV	2V-POPE-Ca^{2+}-SysVI
I	25.61 ± 0.43	26.70 ± 0.68	28.90 ± 1.24	25.40 ± 1.18	30.81 ± 1.55
II	22.78 ± 0.32	23.17 ± 0.67	24.66 ± 0.73	19.77 ± 0.33	24.29 ± 0.78
III	24.77 ± 0.20	21.92 ± 0.22	22.30 ± 0.15	18.26 ± 0.49	21.90 ± 0.21
IV	22.31 ± 0.23	–	20.69 ± 0.12	–	–
V	–	–	21.18 ± 0.27	–	–

simulations on two reaction coordinates—the values of $SASA_{sum\text{-}in}$ and $SASA_{sum\text{-}out}$—in terms of the potential mean force. We calculated the free energy using the equation

$$\Delta G(q_1, q_2) = -k_B T \ln P(q_1, q_2)$$

where q_1 is the value of $SASA_{sum\text{-}out}$, q_2 is the value of $SASA_{sum\text{-}in}$, and $P(q_1,q_2)$ is a canonical probability distribution function; the lowest free energy was set to zero. Fig. 4 shows the free energy landscape for the 2V–POPE–Ca^{2+}-SysI fusion simulation. The free energy landscapes for other fusion simulations are provided in Figure SI. The vesicle-vesicle fusion event proceeded from the initial state [Fig. 4(a)] having two vesicles bound by inter-vesicle Ca^{2+}–lipid clusters. Fig. 4(b) presents the configuration of the stalk state featuring several lipids of outer leaflets of vesicles connecting two vesicles. Fig. 4c, d, e, and f present the four hemifusion states with various sizes of hemifused diaphragm. Although hemifusion state III is less obvious in the one dimensional energy profile (Fig. 3), it forms an obvious energy basin in this two-dimensional energy landscape. All of the two neighboring hemifusion states are separated by a higher energy basin indicating the formation of the hemifusion diaphragm for the fusion pore is a multi-step event requiring energy input (*e.g.*, thermal energy) for inner lipids to overcome the energy barrier to form a mature hemifusion diaphragm for the fusion pore. From hemifusion states I to IV, the $SASA_{sum\text{-}in}$ values increase indicating the expansion of the hemifusion diaphragm; at the same time, the $SASA_{sum\text{-}in}$ values are also increased indicating the re-organization of the outer leaflets of two fusion vesicle. These results imply that the expansion of hemifusion diaphragm is a collective re-organization of inner and outer lipids. Similar results have been observed for other simulated fusion systems. A fusion pore [Fig. 4(g)] was formed associated with the hemifusion state IV.

3.3. Properties of the hemifusion diaphragm

Table 2 lists the average thickness of hemifusion diaphragms in all hemifused states. The inner lipids of two individual vesicles are considered to form a hemifusion diaphragm when they are in contact. The thickness of a hemifusion diaphragm was calculated as the shortest distance between the phosphorus atom of one lipid in a given leaflet and all of the phosphorus atoms of the lipids in the other leaflet. Therefore, each lipid in one leaflet can define one thickness of hemifusion diaphragm. The average thickness of a hemifusion diaphragm was averaged over the thickness defined by all of the lipids in one leaflet and then averaged over a defined simulation time. The average thickness of the hemifusion diaphragm of all hemifused states for all fusion systems is 23.07 ± 2.51 Å. The calculated thickness of planar POPE lipid bilayers in the presence of Ca^{2+} cations is 43.45 ± 0.87 Å. The thickness of the hemifusion diaphragm of the fusion vesicle is only ~50% of that of planar POPE lipid bilayers. Interestingly, a hemifusion diaphragm thinning effect was observed for the hemifusion pore formation. For a given system (except for 2V-POPE-Ca^{2+}-SysIII), the last hemifused state associated with the pore formation has a thinner hemifusion diaphragm than others. In the 2V-POPE-Ca^{2+}-SysIII, hemifusion diaphragm IV is slightly thicker than hemifusion diaphragm III, nevertheless, hemifusion diaphragms III and IV are less thick than hemifusion diaphragms I and II. To further investigate the structure of the hemifusion diaphragm, we calculated the tail lengths of lipids involved in the hemifusion diaphragm. The calculated tail lengths of lipids [36] are 16.79 ± 0.45 and 16.38 ± 0.47 Å for the *sn-1* and *sn-2* chains, respectively. The tail lengths of lipids involved in the hemifusion diaphragm are only slightly shorter than those of the planar lipid bilayers (18.42 ± 0.41 and 18.10 ± 0.95 Å for the *sn-1* and *sn-2* chains). These results indicate that the thinning of the hemifusion diaphragm does not mainly arise from the shrinkage of lipid tails. By visualizing the

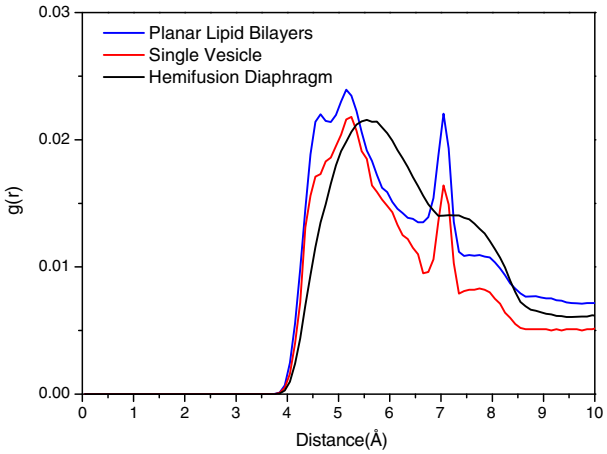

Fig. 6. Radial distribution functions $g(r)$ of phosphorus atoms of the POPE lipids of the hemifusion diaphragm, planar lipid bilayers and a single vesicle.

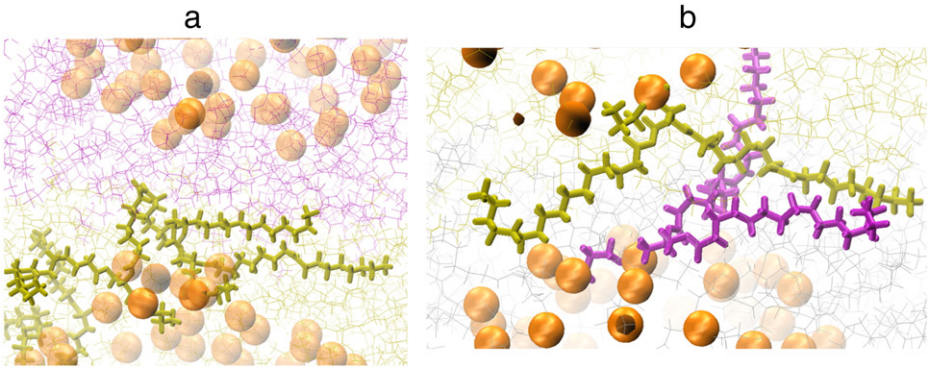

Fig. 5. Snapshots of the structure of the hemifusion diaphragm. (a) Tilting tails of lipids and (b) interdigitated lipid tails. Color code: The head group regions of the hemifusion diaphragm are presented by phosphorus atoms displaying an orange VDW ball; the inner leaflets of two fusing vesicles are presented in licorice style in gold and purple, respectively. The lipids with tilting tails are highlighted.

structure of the simulated hemifusion diaphragm, we observed that the tails of lipids involved in the hemifusion diaphragm are more perpendicular to the hemifusion diaphragm normal [Fig. 5(a)] in contrast to that of more parallel fashion observed in the planar lipid bilayers. Some lipids of two individual leaflets of the hemifusion diaphragm are interdigitated [Fig. 5(b)] and the *Sn-1* and *Sn-2* chains in one lipid are not packed together.

Fig. 6 shows the calculated $g(r)$ of phosphorus atoms of the hemifused diaphragm, planar lipid bilayers and a single vesicle. The first peaks in the distributions $g(r)$ of the hemifused diaphragm were broad, centered at 5.5 Å; the second peak was less obvious. In contrast, the structural features in the distribution $g(r)$ of the planar lipid bilayers and single vesicle were prominent; the first peak is centered at c.a. 5.2 Å and its second peak is sharp, centered at 7.0 Å. These results suggest that the hemifused diaphragm is less structured than the planar lipid bilayers and single vesicles.

4. Conclusions and summary

We have used all-atom MD simulations to simulate membrane fusion in a spontaneous fashion using vesicle models, which were pre-bound by inter-vesicle Ca^{2+}-lipid clusters. The free energy landscape of vesicle fusion and the fusion events during vesicle fusion were investigated. Unlike assumptions made in most continuum models [12–14], our results show the formation of the hemifusion diaphragm for vesicle fusion is a multi-step event, in which each neighboring step is separated by an energy barrier. The expansion of the hemifusion diaphragm requires a collective re-organization of the lipids of the inner and outer leaflets of individual vesicles at the same time. In comparison to planar lipid bilayers, the hemifusion diaphragm is less structured and thinner. The tails of lipids involved in the hemifusion diaphragm are packed in a more perpendicular fashion with respect to the hemifusion diaphragm normal. Hemifusion diaphragm thinning leads to the formation of fusion pore for vesicle fusion. This work provides new insights into the formation of the hemifusion diaphragm, which increase our understanding of membrane fusion.

Acknowledgements

We thank the National Science Council of Taiwan for financial support (grant number: 100-2113-M-008-003-MY2) and the National Center for High-Performance Computing and the V'ger computer cluster at the National Central University of Taiwan for computer time and facilities.

Appendix A. Supplementary data

Supporting information available: Chemical structure of POPE and two-dimensional free energy landscape of fusion simulations. Supplementary data associated with this article can be found, in the online version, at http://dx.doi.org/10.1016/j.bbamem.2014.01.018.

References

[1] R. Jahn, T. Lang, T.C. Südhof, Membrane fusion, Cell 112 (2003) 519–533.
[2] L.V. Chernomordik, M.M. Kozlov, Membrane hemifusion: crossing a chasm in two leaps, Cell 123 (2005) 375–382.
[3] J.C. Shillcock, R. Lipowsky, Tension-induced fusion of bilayer membranes and vesicles, Nat. Mater. 4 (2005) 225–228.
[4] J.M. Warner, B. O'Shaughnessy, The hemifused state on the pathway to membrane fusion, Phys. Rev. Lett. 108 (2012) 178101.
[5] K. Lahdesmaki, O.H. Ollila, A. Koivuniemi, P.T. Kovanen, M.T. Hyvonen, Membrane simulations mimicking acidic pH reveal increased thickness and negative curvature in a bilayer consisting of lysophosphatidylcholines and free fatty acids, Biochim. Biophys. Acta 1798 (2010) 938–946.
[6] P.M. Kasson, V.S. Pande, Control of membrane fusion mechanism by lipid composition: predictions from ensemble molecular dynamics, PLoS Comput. Biol. 3 (2007) e220.
[7] A. Portis, C. Newton, W. Pangborn, D. Papahadjopoulos, Studies on the mechanism of membrane fusion: evidence for an intermembrane calcium(2+) ion-phospholipid complex, synergism with magnesium(2+) ion, and inhibition by spectrin, Biochemistry 18 (1979) 780–790.
[8] H.H. Tsai, W.F. Juang, C.M. Chang, T.Y. Hou, J.B. Lee, Molecular mechanism of Ca-catalyzed fusion of phospholipid micelles, Biochim. Biophys. Acta 1828 (2013) 2729–2738.
[9] Z.K. Issa, C.W. Manke, B.P. Jena, J.J. Potoff, $Ca2^{+}$ bridging of apposed phospholipid bilayers, J. Phys. Chem. B 114 (2010) 13249–13254.
[10] Z.D. Schultz, I.M. Pazos, F.K. McNeil-Watson, E.N. Lewis, I.W. Levin, Magnesium-induced lipid bilayer microdomain reorganizations: implications for membrane fusion, J. Phys. Chem. B 113 (2009) 9932–9941.
[11] J. Zimmerberg, L.V. Chernomordik, Membrane fusion, Adv. Drug Deliv. Rev. 38 (1999) 197–205.
[12] P.M. Kasson, N.W. Kelley, N. Singhal, M. Vrljic, A.T. Brunger, V.S. Pande, Ensemble molecular dynamics yields submillisecond kinetics and intermediates of membrane fusion, Proc. Natl. Acad. Sci. 103 (2006) 11916–11921.
[13] S.J. Marrink, A.E. Mark, The mechanism of vesicle fusion as revealed by molecular dynamics simulations, J. Am. Chem. Soc. 125 (2003) 11144–11145.
[14] V. Knecht, S.-J. Marrink, Molecular dynamics simulations of lipid vesicle fusion in atomic detail, Biophys. J. 92 (2007) 4254–4261.
[15] S.J. Marrink, A.H. de Vries, D.P. Tieleman, Lipids on the move: simulations of membrane pores, domains, stalks and curves, Biochim. Biophys. Acta 1788 (2009) 149–168.
[16] Y.G. Smirnova, S.J. Marrink, R. Lipowsky, V. Knecht, Solvent-exposed tails as prestalk transition states for membrane fusion at low hydration, J. Am. Chem. Soc. 132 (2010) 6710–6718.
[17] P.M. Kasson, E. Lindahl, V.S. Pande, Atomic-resolution simulations predict a transition state for vesicle fusion defined by contact of a few lipid tails, PLoS Comput. Biol. 6 (2010) e1000829.
[18] Y. Kozlovsky, M.M. Kozlov, Stalk model of membrane fusion: solution of energy crisis, Biophys. J. 82 (2002) 882–895.
[19] Y. Kozlovsky, A. Efrat, D.P. Siegel, M.M. Kozlov, Stalk phase formation: effects of dehydration and saddle splay modulus, Biophys. J. 87 (2004) 2508–2521.
[20] P.I. Kuzmin, J. Zimmerberg, Y.A. Chizmadzhev, F.S. Cohen, A quantitative model for membrane fusion based on low-energy intermediates, Proc. Natl. Acad. Sci. 98 (2001) 7235–7240.
[21] A. Grafmüller, J. Shillcock, R. Lipowsky, Pathway of membrane fusion with two tension-dependent energy barriers, Phys. Rev. Lett. 98 (2007) 218101.
[22] S.J. Marrink, A.E. Mark, Molecular dynamics simulation of the formation, structure, and dynamics of small phospholipid vesicles, J. Am. Chem. Soc. 125 (2003) 15233–15242.
[23] W.L. Jorgensen, J. Chandrasekhar, J.D. Madura, R.W. Impey, M.L. Klein, Comparison of simple potential functions for simulating liquid water, J. Chem. Phys. 79 (1983) 926–935.
[24] H.-H. Tsai, J.-B. Lee, J.-M. Huang, R. Juwita, A molecular dynamics study of the structural and dynamical properties of putative arsenic substituted lipid bilayers, Int. J. Mol. Sci. 14 (2013) 7702–7715.
[25] H.H. Tsai, W.X. Lai, H.D. Lin, J.B. Lee, W.F. Juang, W.H. Tseng, Molecular dynamics simulation of cation–phospholipid clustering in phospholipid bilayers: possible role in stalk formation during membrane fusion, Biochim. Biophys. Acta 1818 (2012) 2742–2755.
[26] J.B. Klauda, R.M. Venable, J.A. Freites, J.W. O'Connor, D.J. Tobias, C. Mondragon-Ramirez, I. Vorobyov, A.D. MacKerell, R.W. Pastor, Update of the CHARMM all-atom additive force field for lipids: validation on six lipid types, J. Phys. Chem. B 114 (2010) 7830–7843.
[27] L. Kale, R. Skeel, M. Bhandarkar, R. Brunner, A. Gursoy, N. Krawetz, J. Phillips, A. Shinozaki, K. Varadarajan, K. Schulten, NAMD2: greater scalability for parallel molecular dynamics, J. Comput. Phys. 151 (1999) 283–312.
[28] S.E. Feller, Y.H. Zhang, R.W. Pastor, B.R. Brooks, Constant-pressure molecular-dynamics simulation — the Langevin piston method, J. Chem. Phys. 103 (1995) 4613–4621.
[29] P.J. Steinbach, B.R. Brooks, New spherical-cutoff methods for long-range forces in macromolecular simulation, J. Comput. Chem. 15 (1994) 667–683.
[30] J.-P. Ryckaert, G. Ciccotti, H.J.C. Berendsen, Numerical integration of the cartesian equations of motion of a system with constraints: molecular dynamics of n-alkanes, J. Comput. Phys. 23 (1977) 327–341.
[31] B. Lee, F.M. Richards, The interpretation of protein structures: estimation of static accessibility, J. Mol. Biol. 55 (1971) 379-IN374, 379–400.
[32] W. Humphrey, A. Dalke, K. Schulten, VMD: visual molecular dynamics, J. Mol. Graph. 14 (1996) 33–38.
[33] L.V. Chernomordik, M.M. Kozlov, Mechanics of membrane fusion, Nat. Struct. Mol. Biol. 15 (2008) 675–683.
[34] K.N. Burger, Greasing membrane fusion and fission machineries, Traffic 1 (2000) 605–613.
[35] B.A. Joughin, B. Tidor, M.B. Yaffe, A computational method for the analysis and prediction of protein: phosphopeptide-binding sites, Protein Sci. 14 (2005) 131–139.
[36] The tail length of sn-1 chain is the distance from C2 to C316 and the tail length of sn-s chain is the distance from C2 to C218.